Published in final edited form as:
Neurobiol Dis. 2009 September ; 35(3): 415–425. doi:10.1016/j.nbd.2009.06.004.

Brainstem Alzheimer's-Like Pathology in the Triple Transgenic Mouse Model of Alzheimer's Disease

Cassia R. Overk, **Christy M. Kelley**, and **Elliott J. Mufson**
Department of Neurological Sciences, Rush University Medical Center, Chicago, IL 60612

Abstract

The triple transgenic mouse (3xTgAD), harboring human APP_{Swe}, $PS1_{M146V}$ and Tau_{P301L} genes, develops age-dependent forebrain intraneuronal Aβ and tau and extraneuronal plaques. We evaluated brainstem AD-like pathology using 6E10, AT8, and Alz50 antibodies and unbiased stereology in young and old 3xTgAD mice. Intraneuronal Aβ occurred in the tectum, periaqueductal gray, substantia nigra, red nucleus, tegmentum and mesencephalic V nucleus at all ages. Aβ-positive neuron numbers significantly decreased in the superior colliculus and substantia nigra while AT8-positive superior colliculus, red nucleus, principal sensory V, vestibular nuclei, and tegmental neurons significantly increased between 2 and 12 months. Alz50-positive neuron numbers increased only in the inferior colliculus between these ages. Dual labeling revealed a few Aβ- and tau- positive neurons. Plaques occurred only in the pons of female 3xTgAD mice starting at 9 months. 3xTgAD mice provide a platform to define *in vivo* mechanisms of Aβ and tau brainstem pathology.

Keywords

Alzheimer's disease; amyloid; brainstem; pathology; stereology; tau; transgenic

Introduction

Although the brains of patients with Alzheimer's disease (AD) are characterized by the presence of neurofibrillary tangles (NFT) and beta-amyloid (Aβ) plaques, the distribution and disease-related progression of these lesions has mainly been detailed in the neo and limbic cortex (Bancher et al. 1993; Braak et al. 1991; Schonheit et al. 2004; Thal et al. 2002). On the other hand, the distribution of brainstem AD-like pathology is not well defined despite the fact that nearly 50 % of AD cases display lesions in non-telencephalic areas of the brain (Thal et al. 2002). The AD brainstem exhibits neurofibrillary tangles in the inferior colliculus (Ohm et al. 1989; Sinha et al. 1993a), locus coeruleus (Chan-Palay et al. 1990), pedunculopontine nucleus (Mufson et al. 1988), dorsal raphe (Aletrino et al. 1992; Curcio et al. 1984), and substantia nigra (Schneider et al. 2002). Cell loss is documented in Edinger-Westphal neurons (Scinto et al. 2001), and Aβ plaque pathology is seen in the

Address correspondence to: Elliott J. Mufson, Ph.D., Professor of Neurological Sciences, Alla V. and Solomon Jesmer Chair in Aging, Rush University Medical Center, 1735 W. Harrison Street, Suite 300, Chicago, IL 60612, 312-563-3558 tel., 312-563-3571 fax., emufson@rush.edu .

substantia nigra, periaqueductal gray, superior and inferior colliculi, and red nucleus (Brilliant et al. 1992; Iseki et al. 1989; Parvizi et al. 2001; Thal et al. 2002).

Animal models that mimic the distribution of AD-like pathology are important tools in the investigation of the pathogenesis of Aβ and neurofibrillary lesions. The vast majority of mouse models of AD have been generated by incorporating familial AD (FAD) mutations of the amyloid precursor protein (APP) and/or presenilin-1 (PS1) gene into the mouse genome resulting in extensive age-dependent brain Aβ plaque pathology (Games et al. 2006). Most studies using Aβ-over-expressing mice have concentrated on understanding the distribution and progression of Aβ plaques in the cerebral and limbic cortices (Borchelt et al. 1997; Gordon et al. 2002; Holcomb et al. 1998; Hsiao et al. 1996; Jaffar et al. 2001; Wengenack et al. 2000), whereas only a few studies have reported brainstem Aβ plaque pathology (Christensen et al. 2008a). By contrast, mice over-expressing the human tau gene, P301L, alone and in combination with APP FAD genes, display forebrain and brainstem tangle-like structures (Gotz et al. 2001; Lewis et al. 2001; Lewis et al. 2000; Ramsden et al. 2005; Santacruz et al. 2005). Recently, LaFerla and coworkers developed a triple transgenic mouse (3xTgAD) harboring human APP_{Swe}, $PS1_{M146V}$ and Tau_{P301L} gene mutations (Oddo et al. 2003b), which develops intraneuronal Aβ and tau, as well as Aβ plaques in an age-dependent manner within the cortex, hippocampus and amgydala (Caccamo et al. 2006; Carroll et al. 2007; Oddo et al. 2003a; Oddo et al. 2003b). In the 3xTgAD mouse, three transgenes were subcloned into the Thy1.2 cassette which restricts transgene expression to neurons (Caroni 1997). A review of the literature failed to reveal any mention of brainstem Aβ or tau-like pathology in 3xTgAD mice. In the present study, we evaluated brainstem AD-like pathology using antibodies against Aβ and tau epitopes combined with unbiased stereological counting procedures in young, middle and old 3xTgAD mice.

Material and Methods

Animals

A colony of 3xTgAD and non-transgenic (ntg) mice was generated from breeding pairs provided by Dr. Frank LaFerla from the University of California Irvine. Mice were housed in plastic cages; food and water were available *ad libitum* and animals were maintained on a 12:12-hour light:dark cycle. All animal care and procedures were conducted with approved institutional animal care protocols and in accordance with the NIH Guide for the Care and Use of Laboratory Animals. Three male and three female mice at 2, 6, 9, or 12 months of age were deeply anaesthetized with ketamine/xylazine (95 and 5 mg/kg body weight, respectively) and perfused transcardially with cold physiological saline (pH 7.4), followed by 4 % paraformaldehyde and 0.1 % glutaraldehyde in 0.1 M phosphate-buffered saline (PBS; pH 7.4). Brains were removed from the skull and placed in the same fixative for 24 h and then cryoprotected in 30 % sucrose in PBS at 4 °C for at least 24 h. Coronal brain sections were cut frozen on a sliding knife microtome at 40 μm thickness into six adjacent series and stored at 0 °C in a cryoprotectant solution (30 % ethylene glycol, 30 % glycerol, in 0.1 M PBS) prior to processing.

Immunohistochemistry

Free-floating sections were immunohistochemically processed using antibodies directed against Aβ/APP (6E10; Covance, NJ; 1:2000), the tau conformational marker, Alz50 (gift from Peter Davies, Albert Einstein College of Medicine, Bronx, NY; 1:10,000), and the phospho-specific (Ser202/Thr205) tau antibody AT8 (ThermoFisher; Waltham, MA; 1:1000). Briefly, sections were rinsed in phosphate buffer (PB), washed in Tris-buffered saline (TBS; pH 7.4), incubated in TBS containing sodium meta-periodate (0.1 M; 20 min), rinsed for 30 minutes in a solution containing TBS and Triton X-100 (0.25 %; TBST) and

then blocked in TBST with 3 % goat serum for 1 h. Sections were subsequently incubated with primary antibody in TBST containing 1 % goat serum over-night at room temperature with constant agitation. After several washes in TBS containing 1 % goat serum, sections were incubated with secondary antibody (1:200) in TBS (goat anti-mouse IgG for 6E10 and AT8, or goat anti-mouse IgM for Alz50) with 1 % goat serum at room temperature for 1 h. Sections were washed with TBS and incubated with avidin-biotin complex (1:500; "Elite Kit," Vector Labs). Tissue was then washed in sodium acetate trihydrate (0.2 M) and imidazole (1.0 M) solution (pH 7.4 with acetic acid). Reaction products were visualized using an acetate-imidazole buffer containing 0.05 % 3/3′-diaminobenzidine tetrahydrochloride (DAB; Sigma, MO) and 0.0015 % freshly prepared H_2O_2. Sections were washed in acetate-imidazole buffer to terminate the histochemical reaction, mounted on to alum-submersed slides, air dried for 24 h, dehydrated through a series of graded alcohols (70 %, 95 %, and 100 %), cleared in xylene, and cover-slipped with DPX. Sections were analyzed at the light microscopic level with the aid of a Zeiss Axioplan 2 microscope.

6E10 and AT8 Dual Immunocytochemistry

Selected sections were double-labeled for 6E10 and AT8 using the above protocol with the following modifications for immunofluorescence. Tissue was incubated with primary antibody overnight (6E10; 1:800). After rinsing, tissue was incubated with a Fab fragment (rabbit anti-mouse; 1:50) for 1 h. Sections were washed and then incubated in a secondary antibody (Cy2 donkey anti-rabbit; 1:400) for 80 min in the dark. Tissue was washed with TBS containing 3 % donkey serum and then incubated in AT8 (1:150) overnight in the dark. Tissue was again rinsed and then incubated in Cy3 donkey anti-mouse secondary antibody (1:400) for 80 min in the dark. Immunofluorescence was visualized using a Zeiss Axioplan 2 microscope using excitation filters at wavelengths 489 and 555 nm and emission filters at 505 and 570 nm for Cy2 and Cy3, respectively. Florescent images were stored on a computer and contrast was enhanced using Adobe Photoshop (Version 7).

6E10 and Glial Fibrillary Acidic Protein (GFAP) Dual Immunocytochemistry

Selected sections were double-labeled for 6E10 and GFAP using the above protocol with the following modifications for immunofluorescence. First, sections were incubated with the GFAP antibody overnight (Dako, CA; 1:2000). After rinsing, tissue was then incubated in a secondary antibody (Cy3 goat anti-rabbit; 1:300) for 120 min in the dark. Tissue was washed with TBS containing 3 % goat serum and then incubated using the 6E10 antibody (1:800) overnight in the dark. Tissue was rinsed and incubated in Cy2 goat anti-mouse secondary antibody (1:300) for 120 min in the dark. Sections were analyzed using the above mentioned microscopy.

Immunohistochemical Controls

In the present investigation, two control immunostaining experiments were undertaken. First, tissue was processed as described above except that the primary antibody was deleted. In virtually all areas examined reactivity was absent with the exception of light intraneuronal labeling in the fifth and seventh motor and deep cerebellar nuclei in sections stained for 6E10 and AT8. Second, to further determine whether the brainstem labeling was specific or due to cross reactivity of the secondary antibody, brainstem sections were reacted using a biotinylated 6E10 (1:2000) or AT8 (1:200) antibody (Covance, NJ). These sections displayed a similar distribution of 6E10 immunoreactive neurons but the seventh motor and the deep cerebellar nuclei were immunonegative suggesting that the cranial and cerebellar nuclear stainings were non-specific. Furthermore, sections reacted with the biotinylated AT8 antibody revealed fewer labeled neurons compared to the visualization using DAB as the chromogen in those areas of the brainstem examined with the exception of the fifth and seventh motor nuclei and cerebellar nuclei at all ages. However, AT8-positive neurites

similar to those seen in sections reacted with DAB were observed within the motor nucleus of V. It should be noted that the specificity for the antibodies used, as is the case for all peptides, is not absolute. It is possible that the antiserum reacted with a structurally related protein. Therefore, a degree of caution, which is inherent to immunohistochemical procedures, is warranted. In this regard immunoreactivity refers to "-like" immunoreactivity in this report.

Unbiased Stereology

Stereological methods were used to estimate the number of neurons immunoreactive for 6E10, AT8, or Alz50 utilizing an optical fractionator unbiased sampling design using 2 and 12 month old 3xTgAD mice as previously described (Jaffar et al. 2001; Perez et al. 2005). A total of 10 alternating brainstem sections separated by approximately 480 μm containing the superior colliculus, inferior colliculus, red nucleus, substantia nigra pars compacta, pontine nuclei, motor nucleus of V, principal sensory nucleus of V, vestibular nucleus, spinal nucleus of V, and the reticular area were outlined bilaterally using a 4x objective attached to an Olympus BX51 microscope. Although stereological data were collected for 6E10- and Alz50-immunoreactive (ir) neurons in the motor nucleus of V, these data were not collected for AT8-ir perikarya in the same region due to limited staining. Anatomical nomenclature was based on Paxinos and Franklin (Paxinos et al. 2001). A systematic sampling of the outlined areas was made from a random starting point using StereoInvestigator 8.21.1 software (Micro-BrightField, Cochester, VT). Counts were taken at predetermined intervals (x = 221, y = 221), and a counting frame (70 × 70 μm = 4900 μm^2) was superimposed on the live image of the tissue sections. Sections were analyzed using a 60 × 1.4 PlanApo oil-immersion objective with a 1.4 numerical aperture. Section thickness was determined by focusing on the top of the section, zeroing the z-axis and focusing on the bottom of the section. Average section thickness was 16.3 μm with a range of 13.4-18.7 μm. The dissector height was set at 10 μm. This allowed for a 2-μm top guard zone and at least a 2-μm bottom guard zone. The forbidden zones were never included in the cell counting. Immunoreactive neurons were only counted if the first recognizable profile came into focus within the counting frame. This method allowed for a uniform, systematic, and random design. Focusing through the Z-axis revealed that the 6E10 and AT8 antibodies penetrated the full depth of each section. By contrast, the Alz50 antibody penetrated at minimum through the upper 12-μm of each section analyzed by stereology.

Data Analysis

Differences in stereologic counts were evaluated using the Mann-Whitney test for median differences (GraphPad Prism 4.0c for Macintosh, San Diego, CA). The level of statistical significance was set at p-value < 0.05.

Results

Light microscopic evaluation of tissue immunoreacted for 6E10, Alz50, and AT8 revealed intraneuronal staining extending rostrally from the midbrain at the level of the superior colliculus, and caudally to the pontomedullary region, in male and female 3xTgAD mice at each age examined (Figs. 1 and 2). Sections dual stained for GFAP and 6E10 confirmed the neuronal nature of the staining at all ages in the brain region (Fig 3). Immunohistochemical controls failed to reveal staining when the primary antibody was removed (Fig. 4B), nor were ntg mice immunoreactive for any examined antibody (Fig. 4D). At 2 months of age, 6E10-ir round or multipolar neurons were scattered within the superior colliculus (Fig. 1A, B and Fig. 4A). 6E10 interneuronal immunoreactivity displayed a granular cytoplasmic appearance, which gave the appearance of a darkly stained reaction product within the perikarya (Fig. 5J). Scattered 6E10-ir neurons were also seen within the periaqueductal gray,

substantia nigra, red nucleus and tegmentum at this level of the midbrain (Fig. 1 A, B). A cluster of small oval-shaped 6E10-ir neurons was observed within the ventrolateral transition between the superior and inferior colliculus (Fig. 1B). In addition, 6E10-ir neurons were scattered throughout the central portion of the inferior colliculus (Fig. 1C). Within the pontomedullary junction, 6E10-ir neurons were found within the mesencephalic nucleus of V (Figs. 1C, D and 4C, 5A), principal sensory and motor nuclei of V (Figs. 1C and 4C) as well as within the midbrain tegmentum and pons (Fig. 1B - D). Although neuronal dendritic processes of the mesencephalic nucleus of V exhibited 6E10-ir at 2 months, they were immunonegative at 12 months of age in 3xTgAD mice (Fig. 5A, D).

Tissue immunostained for Alz50, a tau conformational marker, or AT8, a tau phosphorylational marker, revealed reduced neuronal staining compared to 6E10 within the brainstem at any age examined. A few AT8 and Alz50-ir neurons were scattered within the superior and inferior colliculi (Fig. 1E-G, I-K). Many more AT8-ir neurons were seen in the red nucleus, substantia nigra, sensory nucleus of V, as well as in the tegmentum (Fig. 1E-H) compared to Alz50 positive neurons in these brainstem regions (Fig. 1I-L). Although the neurons of the mesencephalic nucleus of V were 6E10 and AT8-ir, they were Alz50 immunonegative at all evaluated ages (Fig. 5A-F). Dual immunofluorescence revealed a few 6E10 and AT8 double immunopositive neurons in the superior colliculus (Fig. 5M-O) and mesencephalic nucleus of V (Fig. 5G-I), independent of age and gender. Although not all 6E10-ir neurons were AT8-positive, all AT8-ir neurons were 6E10-ir (Fig. 5G-I; M-O). Many labeled neurons showed age-dependent morphological changes ranging from a loss of dendritic processes to a shrunken appearance with increased intracellular cytoplasmic labeling (Fig. 5J-L; 6).

Brainstem plaque deposition in 3xTgAD mice

A few 6E10 (Aβ/APP)-ir plaques were only seen within the ventral pons beginning at 9 mos of age in female but not male 3xTgAD mice (Fig.7). By 12 months of age, female transgenic mice exhibited many more 6E10-ir plaques than was seen at 9 months of age (Fig.7B, C). 6E10-ir plaques were also reactive for thioflavin-S and AT8, but not Alz50 at these ages (data not shown).

Stereologic analysis of brainstem Aβ and tau-positive neurons in 3xTgAD mice

Unbiased stereologic counts were performed on every 12th section containing the superior colliculus, red nucleus, substantia nigra, inferior colliculus, mesencephalic nucleus of V, pontine nuclei, motor nucleus of V, principal sensory nucleus of V, vestibular nuclei, and the reticular area. Counts revealed that the superior colliculus contained the highest number of 6E10-ir neurons followed by the inferior colliculus, reticular area, red nucleus, pontine region, substantia nigra, vestibular nuclei, principal sensory nucleus of V, mesencephalic nucleus of V, and motor nucleus of V, in descending order. There was an age-related decrease in 6E10-ir neuron numbers in most regions examined; however, only the superior colliculus and the substantia nigra had a statistically significant reduction in 6E10-ir neuron numbers between 2 and 12 months of age (p-value <0.05) (compare Figs. 1 and 2 and 8A). While the reduction in 6E10-ir neurons in the superior colliculus was observed at 6 mos (Fig. 6), the diminution in labeled substantia nigra perikarya was evident at 9 months of age (Fig. 6).

Although there was a trend toward an age-related increase in AT8-ir neuron number in the brainstem regions examined, only the superior colliculus, red nucleus, principal sensory of V, vestibular nuclei, and reticular area differed significantly between 2 and 12 months of age (p-value <0.05; Fig. 8B). By contrast, Alz50 immunolabeling revealed the least number of neurons in the brainstem areas examined compared to 6E10 and AT8. The superior and

inferior colliculi exhibited the greatest number of Alz50-ir neurons (Fig. 8C). The inferior colliculus was the only brainstem region to show a statistically significant increase in Alz50-ir neurons (p-value <0.05) between 2 and 12 months of age in 3xTgAD mice (Fig. 8C).

Discussion

To our knowledge, the present findings are the first demonstration of 6E10 (Aβ/APP), AT8 and Alz50 intraneuronal immunoreactivity in the brainstem of young and old 3xTgAD mice. These findings extend the observation of intraneuronal Aβ- and tau-positive neurons seen in the forebrain of 3xTgAD mice (Caccamo et al. 2006; Carroll et al. 2007; Oddo et al. 2003a; Oddo et al. 2003b). 6E10- and AT8-ir plaques were only seen in the pontine gray matter of the brainstem in female 3xTgAD mice.

APP/Aβ (6E10) and tau brainstem pathology in 3xTgAD mice

The current demonstration of 6E10-immunoreactive brainstem neurons is in contrast to other mutant mice over-expressing the FAD $APP_{swe}/PS1_{M146L}$ genes, which are similarly found within the 3xTgAD mouse genome. These bigenic mice only display Aβ plaques in the brainstem (Jaffar et al. 2001), whereas we found intraneuronal Aβ labeling in the superior and inferior colliculi, pontine nuclei, vestibular nuclei, spinal trigeminal nucleus and substantia nigra. Therefore, it is likely that the inclusion of the tau_{P301L} gene with the $APP_{swe}/PS1_{M146L}$ genes in the mouse genome drives the intracellular expression of Aβ. However, a recent report describes intracellular Aβ staining in the fifth and seventh motor nuclei in APP/PS1K1 bigenic mice at 12 months of age (Christensen et al. 2008a). In the present study, Aβ immunoreactivity was not found in neurons of the seventh motor nucleus suggesting that different transgenes induce different expression patterns. Perhaps the use of different Aβ antibodies between studies as well as genotype and promoters used to over-express the transgenes underlie the differences between studies. It is intriguing that brainstem areas containing intraneuronal Aβ pathology in 3xTgAD mice are similar to regions that exhibit Aβ plaques in the human AD brain. For example, plaques are seen in the superior and inferior colliculi (Ohm et al. 1989; Parvizi et al. 2001; Sinha et al. 1993a), reticular formation and substantia nigra (Brilliant et al. 1992; Iseki et al. 1989) in sporadic AD, as well as in the red nucleus and vestibular nuclei in familial AD (Brilliant et al. 1992; Iseki et al. 1989). The present findings together with those derived from human AD neuropathology investigations suggest that select brainstem regions are vulnerable to the pathological processes driving the development of AD lesions in both 3xTgAD mice and the human AD brain.

Although the present investigation is the first report of intraneuronal AT8 and Alz50, markers of pretangle formation in the brainstem of 3xTgAD mice, other mouse models of AD neuronal pathology, produced by over-expressing the tau_{P301L} human gene, display NFT-like structures in the brainstem reticular formation, motor nucleus of V, and deep cerebellar nuclei (Lewis et al. 2000), as well as tau gene expression within the superior colliculus (Santacruz et al. 2005). In the human AD condition, NFTs positive for AT8 and Alz50 appear in the superior and inferior colliculi (Parvizi et al. 2001), reticular formation and substantia nigra (Brilliant et al. 1992; Iseki et al. 1989). Ultra-structural analysis of tau_{P301L}-positive neurons revealed a filamentous phenotype similar to that seen in NFTs in the human AD brain (Lewis et al. 2000). In a separate set of ultra-structural experiments performed in our laboratory neither straight nor paired helical filaments were seen in hippocampal or neocortical Alz50- or AT8-ir neurons in 2 and 9 month old 3xTgAD mice, however, straight filaments were observed at 23 months (Oh et al. in preparation);). Factors other than the accumulation of tau proteins in neurons may underlie the filamentous tangle-bearing phenotype seen in AD. For example, differences in the abundance or ratio of specific tau proteins in different cohorts of neurons and/or minor alterations in proteases,

kinases, and phosphatases that alter the structure of these proteins during the life span of the neuron may influence the formation of AD filaments (Conrad et al. 2007; Ginsberg et al. 2006; Goedert et al. 1989), and/or the promoter system designed for specific transgene expression in particular brain regions. Although tau pathology is not required for neuronal degeneration in the $APP_{swe}/PS1_{\Delta E9}$ (Liu et al. 2008), a significant body of literature supports the concept that tau abnormalities play some role in the neurodegeneration seen in human AD.

Age-related reduction in brainstem pathology in 3xTgAD mice

Quantitative unbiased counting revealed decreased numbers of 6E10-ir neurons in the superior colliculus and substantia nigra, pars reticulata between 2 and 12 month old 3xTgAD mice. Whether these decreases in 6E10-ir neurons were due to changes in the total number of perikarya or changes in phenotype is unclear. There is evidence that during the course of AD, cholinergic forebrain neuron numbers are stable, but there is a phenotype down-regulation for the expression of specific neurotrophic receptor proteins in these perikarya during the early stages of AD (Counts et al. 2005). Recently, Oddo et al. used dot blots to show decreased Aβ oligomer levels in the hippocampal/subicular complex at 6 and 12 months of age in 3xTgAD mice (Oddo et al. 2006). While the mechanism(s) underlying this decrease remains unclear, it was hypothesized that increased Aβ fibrillarization led to decreased amounts of Aβ oligomers. It is possible that an increase in Aβ fibrillarization is also occurring in the brainstem; however, since the 6E10 antibody does not differentiate between Aβ species, stereological counts revealed a total decrease in APP/Aβ species at 12 months compared to 2 months. Moreover, our finding of a decrease in intraneuronal Aß in the superior collicullus and lend support to studies showing that intraneuronal Aβ increases until extracellular Aβ deposits form, at which point intraneuronal Aβ levels decrease in transgenic animal models of amyloidosis (Christensen et al. 2008b; Langui et al.,2004; Lord et al. 2006) and Downs syndrome (Mori et al. 2002). On the other hand, AT8-ir neuron numbers increased in the superior colliculus, red nucleus, principal sensory of V, vestibular nuclei and reticular formation during the same time period. Compared to the number of AT8-ir neurons, Alz50 revealed many fewer immunoreactive neurons in the brainstem regions examined. This differential staining pattern is likely due to the observation that Alz50 identifies a tau conformational change that occurs later than the phosphorylational state identified by AT8 (Luna-Munoz et al. 2007).

Functional implications of brainstem AD-like pathology in 3xTgAD mice

The functional consequences of brainstem intraneuronal AD-like pathology in 3xTgAD mice remain to be determined. AD-like pathology in the motor nucleus of V and vestibular nucleui suggest deficits in motor behaviors in these mice. Interestingly, mice over-expressing the tau_{P301L} gene alone exhibit deficits in spontaneous hind paw clinching while standing, delayed righting response, loss of ambulation, and difficulty opening their eyes (Lewis et al. 2000). Although motor functions using gait, stepping, and hind limb clasping motor tests were examined in 3xTgAD mice, no data were provided (Billings et al. 2007). Intraneuronal 6E10 in the superior and inferior colliculi suggest impairments in visual and auditory orientating behavior in 3xTgAD mice similar to the human condition (Ohm et al. 1989; Sinha et al. 1993b). Since the red nucleus and neurons within the reticular formation also displayed Aβ and tau labeling it is possible that these mice have locomotor (Lavoie et al. 2002) and/or arousal deficits (Wu et al. 2007).

Brainstem plaque deposition in 3xTgAD mice

A particularly interesting finding in this study is the deposition of Aβ-ir plaques in the ventral portion of the pontine nucleus in female but not male 3xTgAD mice beginning at 9 months of age. The time course for the appearance of plaque deposition in the brainstem is

similar to that reported in the forebrain of 3xTgAD mice (Caccamo et al. 2006; Carroll et al. 2007; Oddo et al. 2003a; Oddo et al. 2003b). Although the mechanism(s) underlying plaque formation is controversial, data suggest that plaque formation is related to the anterograde axonal transport of APP since disconnection of the entorhinal cortex from hippocampus results in the clearance of Aβ deposits in another amyloid over-expressing mouse (Lazarov et al. 2002). This model suggests that afferent inputs to the pontine gray region may provide a substrate for Aβ deposition in the brainstem. Several brainstem regions which innervate the pontine gray displayed 6E10-ir neurons including the lateral portion of the superior colliculus (Burne et al. 1981). The spinal trigeminal nucleus, vestibular nucleus (Swenson et al. 1984), lateral and ventral areas of the red nucleus, and mesencephalic nucleus of V (Border et al. 1986) contained APP/Aβ positive neurons. The mechanism(s) responsible for the deposition of Aβ-ir plaques in female as opposed to male 9-month-old triple transgenic mice is unknown. The most likely explanation for the gender difference is hormone-based, since forebrain AD-like pathology is sex-dependent in 3xTgAD mice (Carroll et al. 2007). Whether similar hormonal influences affect the onset of brainstem AD pathology in triple transgenic mice is under investigation.

In summary, 3xTgAD mice display intraneuronal Aβ and tau within select brainstem nuclei. Interestingly, many of the regions containing AD-like cellular pathology are areas known to contain plaques and NFTs in the human AD brain suggesting neuronal vulnerability towards AD pathology. However, the morphological characteristics of intraneuronal Aβ or tau did not resemble classic plaque and tangle pathology seen with human AD. Collectively, our findings indicate that the 3xTgAD mouse model provides a robust platform to define *in vivo* the mechanisms of Aβ and tau brainstem pathology.

Acknowledgments

We thank Dr. S. Perez for helpful discussions with the interpretation of the data. This work was supported in part by TGAG000257, AG10688, and Shapiro Foundation.

References

Aletrino MA, Vogels OJ, Van Domburg PH, Ten Donkelaar HJ. Cell loss in the nucleus raphes dorsalis in Alzheimer's disease. Neurobiol. Aging. 1992; 13:461–468. [PubMed: 1508296]

Bancher C, Braak H, Fischer P, Jellinger KA. Neuropathological staging of Alzheimer lesions and intellectual status in Alzheimer's and Parkinson's disease patients. Neurosci. Lett. 1993; 162:179–182. [PubMed: 8121624]

Billings LM, Green KN, McGaugh JL, LaFerla FM. Learning decreases A beta*56 and tau pathology and ameliorates behavioral decline in 3xTg-AD mice. J. Neurosci. 2007; 27:751–761. [PubMed: 17251414]

Borchelt DR, Ratovitski T, van Lare J, Lee MK, Gonzales V, Jenkins NA, Copeland NG, Price DL, Sisodia SS. Accelerated amyloid deposition in the brains of transgenic mice coexpressing mutant presenilin 1 and amyloid precursor proteins. Neuron. 1997; 19:939–945. [PubMed: 9354339]

Border BG, Kosinski RJ, Azizi SA, Mihailoff GA. Certain basilar pontine afferent systems are GABA-ergic: combined HRP and immunocytochemical studies in the rat. Brain Res. Bull. 1986; 17:169–179. [PubMed: 2429739]

Braak H, Braak E. Neuropathological stageing of Alzheimer-related changes. Acta Neuropathol. 1991; 82:239–259. [PubMed: 1759558]

Brilliant M, Elble RJ, Ghobrial M, Struble RG. Distribution of amyloid in the brainstem of patients with Alzheimer disease. Neurosci. Lett. 1992; 148:23–26. [PubMed: 1300498]

Burne RA, Azizi SA, Mihailoff GA, Woodward DJ. The tectopontine projection the the rat with comments on visual pathways to the basilar pons. J. Comp. Neurol. 1981; 202:287–307. [PubMed: 6271853]

Caccamo A, Oddo S, Billings LM, Green KN, Martinez-Coria H, Fisher A, LaFerla FM. M1 receptors play a central role in modulating AD-like pathology in transgenic mice. Neuron. 2006; 49:671–682. [PubMed: 16504943]

Caroni P. Overexpression of growth-associated proteins in the neurons of adult transgenic mice. J. Neurosci. Methods. 1997; 71:3–9. [PubMed: 9125370]

Carroll JC, Rosario ER, Chang L, Stanczyk FZ, Oddo S, LaFerla FM, Pike CJ. Progesterone and estrogen regulate Alzheimer-like neuropathology in female 3xTg-AD mice. J. Neurosci. 2007; 27:13357–13365. [PubMed: 18045930]

Chan-Palay V, Jentsch B, Lang W, Höchli M, Asan E. Distribution of neuropeptide Y, C-terminal flanking peptide of NPY and galanin and coexistence with catecholamine in the locus coeruleus of normal human, Alzheimer's dementia and Parkinson's disease brains. Dementia. 1990; 1:18–31.

Christensen DZ, Bayer TA, Wirths O. Intracellular Abeta triggers neuron loss in the cholinergic system of the APP/PS1KI mouse model of Alzheimer's disease. Neurobiol. Aging. 2008a; 10:647–55.

Christensen DZ, Kraus SL, Flohr A, Cotel MC, Wirths O, Bayer TA. Transient intraneuronal A beta rather than extracellular plaque pathology correlates with neuron loss in the frontal cortex of APP/PS1KI mice. Acta Neuropathol. 2008b; 116:647–55. [PubMed: 18974993]

Conrad C, Zhu J, Conrad C, Schoenfeld D, Fang Z, Ingelsson M, Stamm S, Church G, Hyman BT. Single molecule profiling of tau gene expression in Alzheimer's disease. J. Neurochem. 2007; 103:1228–1236. [PubMed: 17727636]

Counts SE, Mufson EJ. The role of nerve growth factor receptors in cholinergic basal forebrain degeneration in prodromal Alzheimer disease. J. Neuropathol. Exp. Neurol. 2005; 64:263–272. [PubMed: 15835262]

Curcio CA, Kemper T. Nucleus raphe dorsalis in dementia of the Alzheimer type: neurofibrillary changes and neuronal packing density. J. Neuropathol. Exp. Neurol. 1984; 43:359–368. [PubMed: 6737007]

Games D, Buttini M, Kobayashi D, Schenk D, Seubert P. Mice as models: transgenic approaches and Alzheimer's disease. J. Alzheimers Dis. 2006; 9:133–149. [PubMed: 16914852]

Ginsberg SD, Che S, Counts SE, Mufson EJ. Shift in the ratio of three-repeat tau and four-repeat tau mRNAs in individual cholinergic basal forebrain neurons in mild cognitive impairment and Alzheimer's disease. J. Neurochem. 2006; 96:1401–1408. [PubMed: 16478530]

Goedert M, Spillantini MG, Jakes R, Rutherford D, Crowther RA. Multiple isoforms of human microtubule-associated protein tau: sequences and localization in neurofibrillary tangles of Alzheimer's disease. Neuron. 1989; 3:519–526. [PubMed: 2484340]

Gordon MN, Holcomb LA, Jantzen PT, DiCarlo G, Wilcock D, Boyett KW, Connor K, Melachrino J, O'Callaghan JP, Morgan D. Time course of the development of Alzheimer-like pathology in the doubly transgenic PS1+APP mouse. Exp. Neurol. 2002; 173:183–195. [PubMed: 11822882]

Gotz J, Chen F, Barmettler R, Nitsch RM. Tau filament formation in transgenic mice expressing P301L tau. J. Biol. Chem. 2001; 276:529–534. [PubMed: 11013246]

Holcomb L, Gordon MN, McGowan E, Yu X, Benkovic S, Jantzen P, Wright K, Saad I, Mueller R, Morgan D, Sanders S, Zehr C, O'Campo K, Hardy J, Prada CM, Eckman C, Younkin S, Hsiao K, Duff K. Accelerated Alzheimer-type phenotype in transgenic mice carrying both mutant amyloid precursor protein and presenilin 1 transgenes. Nat. Med. 1998; 4:97–100. [PubMed: 9427614]

Hsiao K, Chapman P, Nilsen S, Eckman C, Harigaya Y, Younkin S, Yang F, Cole G. Correlative memory deficits, Abeta elevation, and amyloid plaques in transgenic mice. Science. 1996; 274:99–102. [PubMed: 8810256]

Iseki E, Matsushita M, Kosaka K, Kondo H, Ishii T, Amano N. Distribution and morphology of brain stem plaques in Alzheimer's disease. Acta Neuropathol. 1989; 78:131–136. [PubMed: 2546358]

Jaffar S, Counts SE, Ma SY, Dadko E, Gordon MN, Morgan D, Mufson EJ. Neuropathology of mice carrying mutant APP(swe) and/or PS1(M146L) transgenes: alterations in the $p75^{(NTR)}$ cholinergic basal forebrain septohippocampal pathway. Exp. Neurol. 2001; 170:227–243. [PubMed: 11476589]

Langui D, Girardot N, El Hachimi KH, Allinquant B, Blanchard V, Pradier L, Duyckaerts C. Subcellular topography of neuronal Abeta peptide in APPxPS1 transgenic mice. Am. J. Pathol. 2004; 165:1465–1477. [PubMed: 15509518]

Lavoie S, Drew T. Discharge characteristics of neurons in the red nucleus during voluntary gait modifications: a comparison with the motor cortex. J. Neurophysiol. 2002; 88:1791–1814. [PubMed: 12364507]

Lazarov O, Lee M, Peterson DA, Sisodia SS. Evidence that synaptically released beta-amyloid accumulates as extracellular deposits in the hippocampus of transgenic mice. J. Neurosci. 2002; 22:9785–9793. [PubMed: 12427834]

Lewis J, Dickson DW, Lin WL, Chisholm L, Corral A, Jones G, Yen SH, Sahara N, Skipper L, Yager D, Eckman C, Hardy J, Hutton M, McGowan E. Enhanced neurofibrillary degeneration in transgenic mice expressing mutant tau and APP. Science. 2001; 293:1487–1491. [PubMed: 11520987]

Lewis J, McGowan E, Rockwood J, Melrose H, Nacharaju P, Van Slegtenhorst M, Gwinn-Hardy K, Paul Murphy M, Baker M, Yu X, Duff K, Hardy J, Corral A, Lin WL, Yen SH, Dickson DW, Davies P, Hutton M. Neurofibrillary tangles, amyotrophy and progressive motor disturbance in mice expressing mutant (P301L) tau protein. Nat. Genet. 2000; 25:402–405. [PubMed: 10932182]

Liu Y, Yoo MJ, Savonenko A, Stirling W, Price DL, Borchelt DR, Mamounas L, Lyons WE, Blue ME, Lee MK. Amyloid pathology is associated with progressive monoaminergic neurodegeneration in a transgenic mouse model of Alzheimer's disease. J. Neurosci. 2008; 28:13805–13814. [PubMed: 19091971]

Lord A, Kalimo H, Eckman C, Zhang XQ, Lannfelt L, Nilsson LN. The Arctic Alzheimer mutation facilitates early intraneuronal Abeta aggregation and senile plaque formation in transgenic mice. Neurobiol. Aging. 2006; 27:67–77. [PubMed: 16298242]

Luna-Munoz J, Chavez-Macias L, Garcia-Sierra F, Mena R. Earliest stages of tau conformational changes are related to the appearance of a sequence of specific phospho-dependent tau epitopes in Alzheimer's disease. J. Alzheimers Dis. 2007; 12:365–375. [PubMed: 18198423]

Mori C, Spooner ET, Wisniewsk KE, Wisniewski TM, Yamaguch H, Saido TC, Tolan DR, Selkoe DJ, Lemere CA. Intraneuronal Abeta42 accumulation in Down syndrome brain. Amyloid. 2002; 9:88–102. [PubMed: 12440481]

Mufson EJ, Mash DC, Hersh LB. Neurofibrillary tangles in cholinergic pedunculopontine neurons in Alzheimer's disease. Ann. Neurol. 1988; 24:623–629. [PubMed: 3202615]

Oddo S, Caccamo A, Kitazawa M, Tseng BP, LaFerla FM. Amyloid deposition precedes tangle formation in a triple transgenic model of Alzheimer's disease. Neurobiol. Aging. 2003a; 24:1063–1070. [PubMed: 14643377]

Oddo S, Caccamo A, Shepherd JD, Murphy MP, Golde TE, Kayed R, Metherate R, Mattson MP, Akbari Y, LaFerla FM. Triple-transgenic model of Alzheimer's disease with plaques and tangles: intracellular Abeta and synaptic dysfunction. Neuron. 2003b; 39:409–421. [PubMed: 12895417]

Oddo S, Caccamo A, Tran L, Lambert MP, Glabe CG, Klein WL, LaFerla FM. Temporal profile of amyloid-beta (Abeta) oligomerization in an in vivo model of Alzheimer disease. A link between Abeta and tau pathology. J. Biol. Chem. 2006; 281:1599–1604. [PubMed: 16282321]

Ohm TG, Braak H. Auditory brainstem nuclei in Alzheimer's disease. Neurosci. Lett. 1989; 96:60–63. [PubMed: 2648201]

Parvizi J, Van Hoesen GW, Damasio A. The selective vulnerability of brainstem nuclei to Alzheimer's disease. Ann. Neurol. 2001; 49:53–66. [PubMed: 11198297]

Paxinos, G.; Franklin, K. The Mouse Brain in Stereotaxic Coordinates. Academic Press; London: 2001.

Perez SE, Lazarov O, Koprich JB, Chen EY, Rodriguez-Menendez V, Lipton JW, Sisodia SS, Mufson EJ. Nigrostriatal dysfunction in familial Alzheimer's disease-linked APPswe/PS1DeltaE9 transgenic mice. J. Neurosci. 2005; 25:10220–10229. [PubMed: 16267229]

Ramsden M, Kotilinek L, Forster C, Paulson J, McGowan E, SantaCruz K, Guimaraes A, Yue M, Lewis J, Carlson G, Hutton M, Ashe KH. Age-dependent neurofibrillary tangle formation, neuron loss, and memory impairment in a mouse model of human tauopathy (P301L). J. Neurosci. 2005; 25:10637–10647. [PubMed: 16291936]

Santacruz K, Lewis J, Spires T, Paulson J, Kotilinek L, Ingelsson M, Guimaraes A, DeTure M, Ramsden M, McGowan E, Forster C, Yue M, Orne J, Janus C, Mariash A, Kuskowski M, Hyman B, Hutton M, Ashe KH. Tau suppression in a neurodegenerative mouse model improves memory function. Science. 2005; 309:476–481. [PubMed: 16020737]

Schneider JA, Bienias JL, Gilley DW, Kvarnberg DE, Mufson EJ, Bennett DA. Improved detection of substantia nigra pathology in Alzheimer's disease. J. Histochem. Cytochem. 2002; 50:99–106. [PubMed: 11748299]

Schonheit B, Zarski R, Ohm TG. Spatial and temporal relationships between plaques and tangles in Alzheimer-pathology. Neurobiol. Aging. 2004; 25:697–711. [PubMed: 15165691]

Scinto LF, Frosch M, Wu CK, Daffner KR, Gedi N, Geula C. Selective cell loss in Edinger-Westphal in asymptomatic elders and Alzheimer's patients. Neurobiol. Aging. 2001; 22:729–736. [PubMed: 11705632]

Sinha UK, Hollen KM, Rodriguez R, Miller CA. Auditory system degeneration in Alzheimer's disease. Neurology. 1993a; 43:779–785. [PubMed: 8469340]

Sinha UK, Hollen KM, Rodriguez R, Miller CA. Auditory system degeneration in Alzheimer's disease. Neurology. 1993b; 43:779–85. [PubMed: 8469340]

Swenson RS, Kosinski RJ, Castro AJ. Topography of spinal, dorsal column nuclear, and spinal trigeminal projections to the pontine gray in rats. J. Comp. Neurol. 1984; 222:301–311. [PubMed: 6321566]

Thal DR, Rub U, Orantes M, Braak H. Phases of A beta-deposition in the human brain and its relevance for the development of AD. Neurology. 2002; 58:1791–1800. [PubMed: 12084879]

Wengenack TM, Whelan S, Curran GL, Duff KE, Poduslo JF. Quantitative histological analysis of amyloid deposition in Alzheimer's double transgenic mouse brain. Neuroscience. 2000; 101:939–944. [PubMed: 11113343]

Wu HB, Stavarache M, Pfaff DW, Kow LM. Arousal of cerebral cortex electroencephalogram consequent to high-frequency stimulation of ventral medullary reticular formation. Proc. Natl. Acad. Sci. U. S. A. 2007; 104:18292–18296. [PubMed: 17984058]

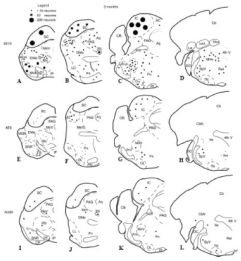

Figure 1.

Schematic drawings showing the distribution of brainstem 6E10, Alz50, or AT8 immunoreactive neurons in 2-month old 3xTg-AD mice. Abr: 3N, third nerve nucleus; 4th V, fourth ventricle; 7N, seventh nerve nucleus; Aq, aqueduct; PAG, periaqueductal gray; Cb, cerebellum; CbN, cerebellar nuclei; CP cerebral peduncle; DMe, deep mesencephalic nucleus; DC, dorsal cochlear nucleus; IC, inferior colliculus; IP, interpeduncular nucleus; LL, lateral lemniscus; MeV, mesencephalic nucleus of V; MGN, medial geniculate; ml, medial lemniscus; MoV, motor nucleus of V; OL, olive; Pn, pontine nuclei; PrV, principal sensory nucleus of V; py, pyramidal tract; RN, red nucleus; SNC, substantia nigra, pars compacta; SNR, substantia nigra pars reticulata; SC, superior colliculus; scp, superior cerebellar peduncle; SpV, spinal trigeminal nucleus of V; Ret, reticular area; Ve, vestibular nuclei.

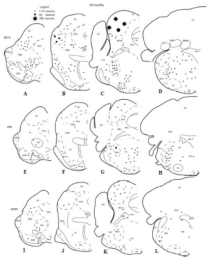

Figure 2.
Schematic drawings showing the brainstem distribution of 6E10, AT8, or Alz50 immunoreactive neurons in 12-month old 3xTg-AD mice. See Figure 1 for anatomical nomenclature.

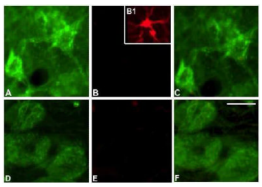

Figure 3.
Photomicrographs of 6E10 (green) and GFAP (red) fluorescent immunoreactive cells in the superior colliculus at 12 months of age (A-C) and mesencephalic nucleus of V (D-F). The inset (B1) is an example of a GFAP immunoreactive glia cell seen in hippocampus. Scale bar = 30 μm.

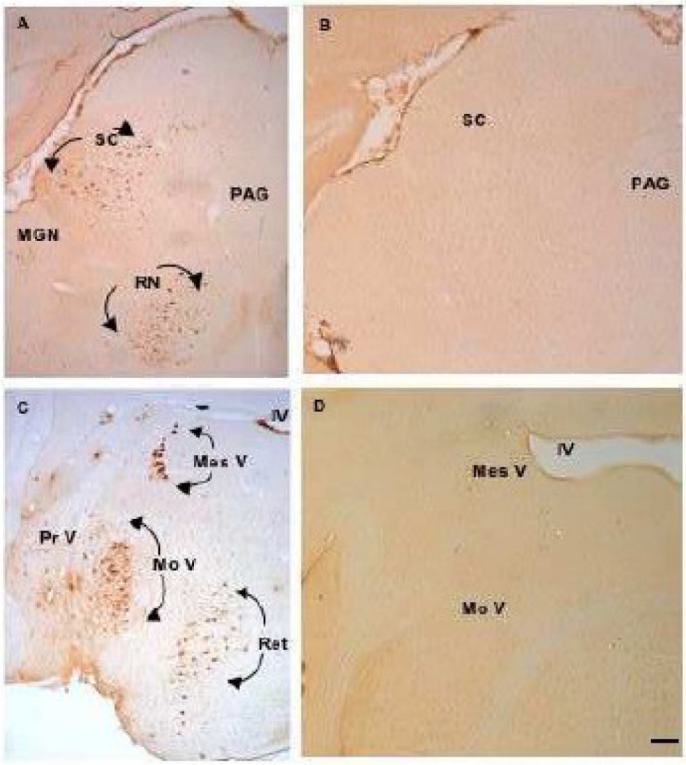

Figure 4.
Low-magnification photomicrographs of 6E10-immunopositive neurons in the superior colliculus (SC) and red nucleus (RN) (A) mesencephalic nucleus of V (mes V), motor nucleus of V (MoV), principal sensory nucleus of V (Pr V), and reticular area (Ret) (C). Section from 3xTgAD brainstem with primary antibody removed (B) and non-transgenic control (D) show absence of immunostaining at the same brainstem levels at 2 months of age. Scale bar = 100 μm.

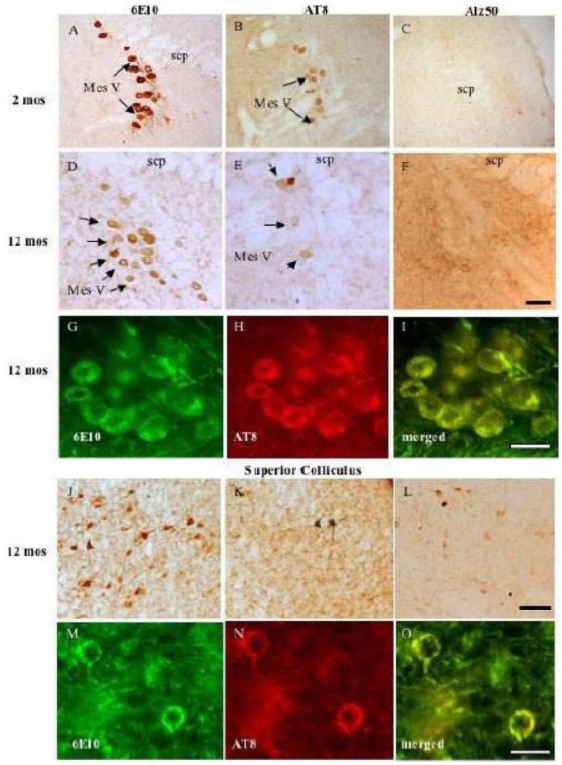

Figure 5.
Photomicrographs of interneuronal 6E10- AT8- and Alz50-immunoreactive neurons in the mesencephalic nucleus of V (mes V) at 2 and 12 months (A-I) and the superior colliculus at 12 mos in 3xTg-AD mice (J-O). At 2 months of age mes V lacked Alz50-ir neurons (C,F). Note co-localization of 6E10 with AT8 in both mes V and superior colliculus (SC) neurons (G-I and M-O). Black scale bar = 100 μm; white scale bar = 50 μm.

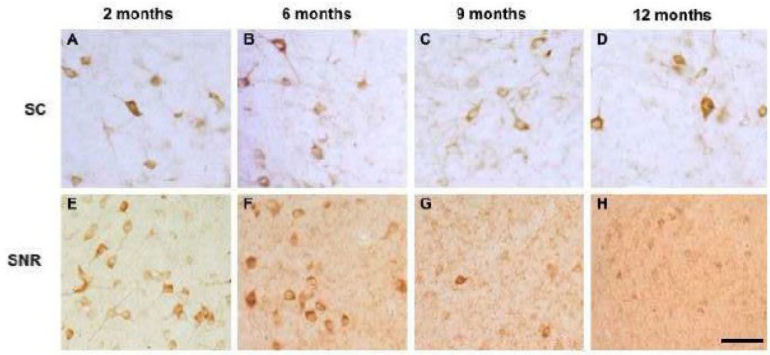

Figure 6.
Photomicrographs showing age-related decrease in 6E10-ir neurons in the superior colliculus (A-D) and substantia nigra (E-G) in 3xTgAD mice. Scale bar = 100 μm.

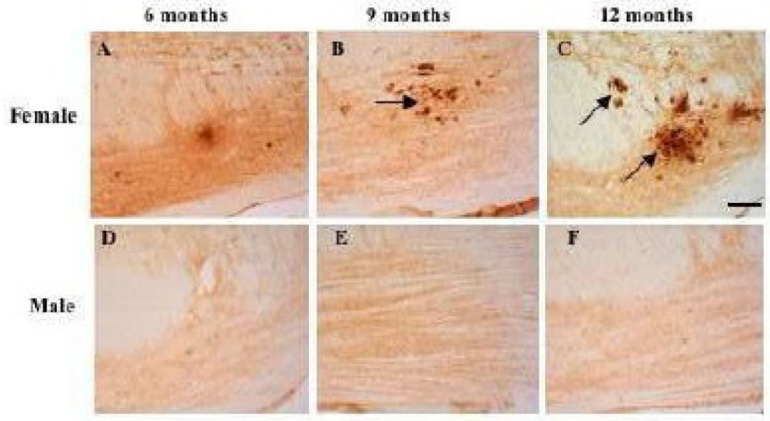

Figure 7.
6E10-positive plaques in the pontine nuclei at 9 and to a greater degree at 12 months in female (A-C), but not in male (D-F) 3xTgAD mice. Scale bar = 100 μm.

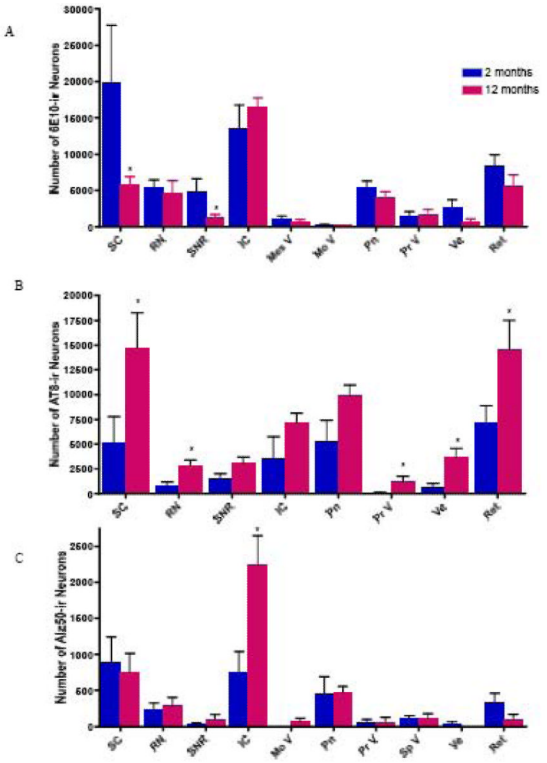

Figure 8.

Histogram showing age-related changes in the number of 6E10-ir (A), AT8-ir (B), and Alz50-ir (C) neurons between 2 and 12 months of age. * p-value < 0.05; Mann-Whitney test.